Detailed high-accuracy megavoltage transmission measurements: A sensitive experimental benchmark of EGSnrc

E. S. M. Ali[a)]
Carleton Laboratory for Radiotherapy Physics, Department of Physics, Carleton University, 1125 Colonel By Drive, Ottawa, Ontario K1S 5B6, Canada

M. R. McEwen[b)]
Ionizing Radiation Standards, Institute for National Measurement Standards, National Research Council, M-35 Montreal Rd, Ottawa, Ontario K1A 0R5, Canada

D. W. O. Rogers[c)]
Carleton Laboratory for Radiotherapy Physics, Department of Physics, Carleton University, 1125 Colonel By Drive, Ottawa, Ontario K1S 5B6, Canada

(Received 17 April 2012; revised 25 June 2012; accepted for publication 27 July 2012; published 12 September 2012)

Purpose: There are three goals for this study: (a) to perform detailed megavoltage transmission measurements in order to identify the factors that affect the measurement accuracy, (b) to use the measured data as a benchmark for the EGSnrc system in order to identify the computational limiting factors, and (c) to provide data for others to benchmark Monte Carlo codes.

Methods: Transmission measurements are performed at the National Research Council Canada on a research linac whose incident electron parameters are independently known. Automated transmission measurements are made on-axis, down to a transmission value of ∼1.7%, for eight beams between 10 MV (the lowest stable MV beam on the linac) and 30 MV, using fully stopping Be, Al, and Pb bremsstrahlung targets and no fattening filters. To diversify energy differentiation, data are acquired for each beam using low-*Z* and high-*Z* attenuators (C and Pb) and Farmer chambers with low-*Z* and high-*Z* buildup caps. Experimental corrections are applied for beam drifts (2%), polarity (2.5% typical maximum, 6% extreme), ion recombination (0.2%), leakage (0.3%), and room scatter (0.8%)—the values in parentheses are the largest corrections applied. The experimental setup and the detectors are modeled using EGSnrc, with the newly added photonuclear attenuation included (up to a 5.6% effect). A detailed sensitivity analysis is carried out for the measured and calculated transmission data.

Results: The developed experimental protocol allows for transmission measurements with 0.4% uncertainty on the smallest signals. Suggestions for accurate transmission measurements are provided. Measurements and EGSnrc calculations agree typically within 0.2% for the sensitivity of the transmission values to the detector details, to the bremsstrahlung target material, and to the incident electron energy. Direct comparison of the measured and calculated transmission data shows agreement better than 2% for C (3.4% for the 10 MV beam) and typically better than 1% for Pb. The differences can be explained by acceptable photon cross section changes of ≤0.4%.

Conclusions: Accurate transmission measurements require accounting for a number of influence quantities which, if ignored, can collectively introduce errors larger than 10%. Accurate transmission calculations require the use of the most accurate data and physics options available in EGSnrc, particularly the more accurate bremsstrahlung angular sampling option and the newly added modeling of photonuclear attenuation. Comparison between measurements and calculations implies that EGSnrc is accurate within 0.2% for relative ion chamber response calculations. Photon cross section uncertainties are the ultimate limiting factor for the accuracy of the calculated transmission data (Monte Carlo or analytical).
[http://dx.doi.org/10.1118/1.4745561]

Key words: transmission measurements, EGSnrc benchmark, photon beams, photonuclear

I. INTRODUCTION

In external photon beams, transmission measurements are a valuable tool to independently extract the photon spectrum and the incident electron energy.[1] However, the problem of extracting spectral information from transmission data is known to be ill-posed because of the weak energy dependence of the attenuation coefficients at therapy energies. This makes the accuracy of the extracted spectral information strongly dependent on the accuracy of the measured transmission signals (among other factors). Despite the large number of experimental transmission measurements in the literature, systematic investigation of influence quantities and their associated uncertainties has been either partial[2–5] or missing. In this study, detailed transmission measurements are performed in which many influence quantities are investigated and corrected for, and a detailed uncertainty budget for the measured signals is constructed. The resulting rigorous estimates of measurement uncertainties are useful when interpreting differences between measured and Monte Carlo-calculated transmission data. They also lead to meaningful confidence bounds on extracted spectral information.[6]

When the incident electron parameters and the setup dimensions are independently known, transmission measurements can be a particularly sensitive primary benchmark of Monte Carlo codes. The increased sensitivity (compared with, e.g., depth–dose measurements) is due to the lack of volume scatter, the extreme attenuation, and the extreme collimation, which collectively amplify small effects that would otherwise be averaged out. Unfortunately for typical clinical linacs the electron parameters are not known accurately, and the head geometry is complex. This is one of the reasons that there are no previous studies that used megavoltage transmission measurements to benchmark a major Monte Carlo code. In this study, measurements are made at the National Research Council (NRC) Canada using a Vickers research linac whose incident electron parameters are independently known, and whose geometry is known and simple. The measured data are used to benchmark the `EGSnrc` system[7,8] and to identify the factors that limit the accuracy of the calculated transmission data.

For the benchmark to be comprehensive, measurements are made down to a transmission value of ~1.7% for a total of eight beams in the range 10–30 MV using bremsstrahlung targets from Be to Pb. For each beam, data are acquired for low-Z and high-Z attenuators using Farmer chambers with low-Z and high-Z buildup caps. The use of multiple attenuators and detectors is to maximize energy differentiation, which makes the benchmark more rigorous. The specific beam energies and attenuator/detector details are chosen such that the final experimental data are suitable as input to another study[6] focused on the unfolding of photon spectra and incident electron energies.

Based on the introduction above, the three goals for this study are: (a) to perform detailed megavoltage transmission measurements in order to identify the factors that affect the measurement accuracy, (b) to use the measured data as a benchmark for the `EGSnrc` system in order to identify the computational limiting factors, and (c) to provide data for others to benchmark Monte Carlo codes. The data needed for the benchmark are available in a web report.[9]

II. MATERIALS AND METHODS

II.A. The NRC Vickers research linac

The NRC Vickers research linac operates at 240 pulses per second, 2.5 μs each. It produces a horizontal pencil beam of nearly monoenergetic electrons, typically within 10–30 MeV. The electron energy is determined by a bending magnet and slit system that was calibrated using a magnetic spectrometer.[10] The bending of the electron beam through the two 45° magnets eliminates photon contamination. The estimated standard uncertainty on the electron energy at the exit window is 0.4%. The electron energy spread is determined from the physical separation of the slits, which is chosen to optimize the two competing demands of beam stability and narrow energy spread. The slit width used in this study leads to an approximately Gaussian energy spread with a standard deviation of 0.4%. The radial spread is known from detailed radiochromic film measurements,[11] and it is approximately Gaussian with a FWHM of 1 mm at the exit window. To determine the beam angular divergence, Ross *et al.*[11] moved the exit window downstream to allow the electron beam to drift an additional 1 m before acquiring film measurements. Their results indicate a small divergence, taken in this study as 0.03° with a virtual apex at 1 m upstream of the exit window. These electron beam parameters are used in the `EGSnrc` model of the setup (Sec. II.E). The exit window is a 41.2 μm Ti alloy (4.42 g/cm^3; 90% Ti, 6% Al, and 4% V, by weight).

In this study, on-axis transmission measurements are made for 10, 15, 20, and 30 MV beams with respective electron energies of 10.09, 15.00/15.70, 20.28, and 30.00 MeV. The 15.70 MeV measurements are used to examine the sensitivity of transmission data to small energy changes, and are used later[6] to confirm the resolving power of the transmission technique in unfolding the incident electron energy. Beams lower than 10 MV (e.g., a 6 MV beam) are not easily attainable on the NRC research linac due to beam instability issues. Bremsstrahlung targets of pure Be, Al, and Pb are placed 2.1 cm downstream of the exit window and cooled by forced air. The target thicknesses are given in Table I and they are sufficient to fully stop the incident electrons. Shielding is added around the targets to reduce stray radiation which contributes to extracameral signals. The resulting photon spectra are soft because of the absence of a flattening filter.

II.B. Transmission measurement setup

The transmission measurement setup is shown in Fig. 1. The narrow-beam geometry starts with a 10.2-cm-thick Pb collimator touching the target shielding (15.0 cm from the exit window), with a nondiverging 1.4-cm-diameter opening. A second 10.2-cm-thick Pb collimator is placed starting at 55.1 cm, with a nondiverging 0.77-cm-diameter opening. Ion chamber measurements behind the second collimator indicate that the leakage through the collimator is ~0.1% of the peak

TABLE I. Thicknesses of the bremsstrahlung targets used in this study (±0.01 cm for Be and Al and ±0.003 cm for Pb). The Be and Al targets are cylindrical with 7.26 cm diameter, and the Pb targets are squares with 3.0 cm side lengths.

Target material	Density (g/cm^3)	Target thickness (cm)			
		10 MV	15 and 15.7 MV	20 MV	30 MV
Be	1.848	–	6.31	–	–
Al	2.699	2.40	3.60	4.31	6.60
Pb	11.35	–	0.793	1.016	–

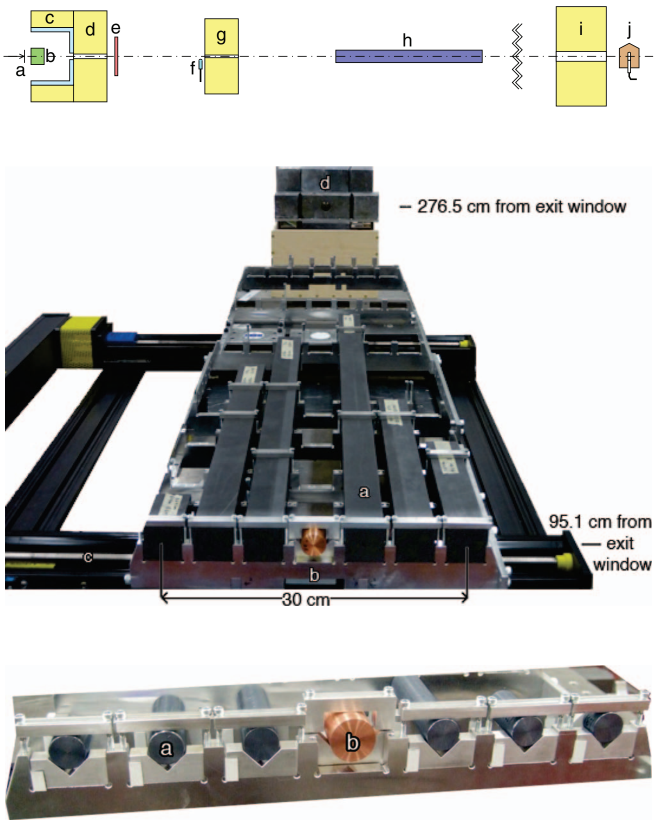

FIG. 1. Top: A schematic of the transmission measurement setup (not to scale) - (a) linac exit window, (b) bremsstrahlung target, (c) target enclosure, (d) first collimator, (e) monitor chamber, (f) field chamber, (g) second collimator, (h) attenuator, (i) third collimator, and (j) Farmer chamber fitted with a buildup cap. Middle: The attenuator assembly - (a) graphite bars, (b) copper benchmark rod (permanently fixed on the assembly), (c) bislide that enables rack movement in the left–right direction, and (d) third collimator. Bottom: (a) Lead attenuator rods and (b) copper benchmark rod.

signal for the highest MV beam. A PTW7862 monitor chamber, operated at a bias of 300 V and connected to a Keithley 6517A electrometer, is used to correct the transmission signals for linac output fluctuations. The chamber consists of four Kapton foils, 50 μm thick each, two of which are coated with graphite of negligible thickness. Its sensitive volume is a central air cylinder of diameter 9.65 cm and thickness 2.4 mm. The monitor chamber is placed between the two collimators (starting at 27.6 cm from the exit window), rather than past the second collimator, to allow for a larger signal and to minimize the variable backscatter contribution which would depend on the presence or absence or an attenuator, and on the attenuator material. No additional buildup material is found to be necessary to provide a reliable monitor signal. An NE2581 chamber with a ^{60}Co buildup cap is used as a field chamber, and the "field-to-monitor" ratio is used throughout the measurements to monitor drifts in the direction of the beam (Sec. II.C). The field chamber is placed downstream of the monitor chamber between the two collimators such that it falls inside the field of the first collimator but outside the field of the second. This makes the field chamber signal more sensitive to the electrons in the direct field (as opposed to only the scatter component) without obstructing the useful beam.

The next component downstream is the attenuators. The low-Z attenuator used is graphite, which has similar attenuation properties to water but allows for a more compact setup and for lower positioning uncertainties. The pure C used[12] is isomolded bars of grade GM10 with a grain size of 10 μm to ensure density uniformity. The ash content is 500 ppm and it is assumed to have typical composition (e.g., Ref. 13), which can be broken down into elements with $Z = 8$, 11, 12, 13, 14, 15, 19, 20, 22, and 26, with respective ppm of 243, 4, 15, 70, 128, 2, 4, 11, 6, and 17. For each MV beam, ten C bar lengths are used (five for each detector) which successively reduce the signal to $\sim$1.7% of its value without an attenuator. The bar lengths are integer multiples of the smallest length—multiples of 8.3 cm for 10 MV, 9.5 cm for 15 MV, and 11.6 cm for 20 and 30 MV, with respective maximum bar lengths of 83.00, 95.00, and 116.00 cm, all $\pm$0.03 cm. The bars have a square cross section of 3.81 cm (1.5 in.) nominal side length, with a milling tolerance of +0.01 in. The extreme case of a +0.01 in. milling error in both side lengths along the full length of a bar would introduce a mass thickness error of $(1.51/1.5)^2 - 1 = 1.3\%$, which would lead to errors of up to 4% in the smallest calculated transmission data. To avoid this, the side lengths of each bar are fully mapped in the two orthogonal directions using a spring-loaded digital caliper gauge (Mitutoyo, Denmark) with a resolution of 20 μm. The data are then used for volume calculations. The mass of the bars is measured using a scale with a resolution of 0.1 g (Sartorius, Germany). In Sec. II.D it is shown that the individual mass thicknesses of the C bars should be used in the Monte Carlo model (rather than the combination of average density and physical lengths). The uncertainty on the individual mass thicknesses is typically 0.07%. The average density (although not used) is 1.728 g/cm^3 with a sample deviation of 0.4%.

The high-Z attenuators are pure Pb rods[14] with maximum impurity of 500 ppm. The typical elemental impurities stated by the supplier are $Z = 12$, 22, 26, 29, 47, 48, 50, and 83 with respective ppm of 1, 5, 2, 20, 20, 2, 70, and 100. Similar to C, ten lengths are used (five per detector) to successively reduce the signal to $\sim$1.7% of its value without an attenuator. The rod lengths are multiples of 0.75 cm for 10 and 15 MV, 0.70 cm for 20 MV, and 0.65 cm for 30 MV, with respective maximum rod lengths of 7.510, 7.000, and 6.510 cm, all $\pm$0.005 cm (note that for a given transmission value, higher MV beams require shorter lengths because the Pb attenuation coefficient has a minimum at $\sim$2.5 MeV). The rods have a diameter of 1.900 $\pm$ 0.001 cm. Unlike C, it is found more accurate for Pb to use the combination of average density and physical lengths because of minor irregularities in the rods (from dents, sagging, etc.). The average density used for all rods is 11.290 g/cm^3, with a sample deviation of 0.15%.

A linear translation system was built to automate the movement of the attenuators. Its base is a motorized Velmex bislide, placed perpendicular to the beam axis. It has a travel of 50.8 cm, and a positioning resolution of 5 μm (200 steps/mm). The base drives a custom Al support rack that has attenuator slots with center-to-center separation of 5 cm. The attenuators are held using multiple small plates with screws that attach to the rack. The additional scatter caused by the translation system and the side attenuators is negligible (Sec. II.C.9). The translation system significantly reduces the overhead time during data acquisition, facilitates more randomized repeats, reduces positioning uncertainties, and reduces the uncertainties from beam instability because beam interruption is reduced by a factor of six. The plane of the front surface of the attenuators is placed at 95.1 cm from the exit window (comparable to a clinical linac isocenter). When the longest C and Pb attenuators are placed in the radiation beam, lateral beam scans downstream did not exhibit any profile horns, confirming that the radiation beam is fully intercepted at the back end of the longest attenuators.

A pure Cu rod of length 2.7 cm and diameter 2.5 cm is permanently fixed in the middle of the translation system. The transmission signal using the Cu rod is acquired many times between the different measurements for a given rack of C or Pb. The "Cu-to-monitor" ratio has two important uses: short-term second-order corrections for drifts in the beam direction (Sec. II.C.4), and long-term monitoring of the stability of the energy of the electron beam (Sec. II.D.2).

Past the attenuator assembly, a third Pb collimator is placed starting at 276.5 cm from the linac exit window. It is 15.3-cm thick, with a nondiverging opening diameter of 2.93 cm (a cone half-angle of 0.29°). It extends ∼15 cm laterally to reduce large-angle scatter into the detector and to reduce cable irradiation which leads to extracameral charge collection.

Transmission signals are acquired using reference-class Farmer chambers. Compared with other detectors previously used, reference-class chambers have a better established history in photon beams (compared with, e.g., parallel-plate chambers[15]), good reproducibility (compared with, e.g., microchambers[16]), very small and quantifiable dose-rate dependence (compared with, e.g., diodes[17]), and dimensions that are suitable for better narrow-beam geometry (compared with, e.g., larger spherical chambers[2,18]). The main chamber used is a 0.6 cc Exradin A19, operating at ±300 V and connected to a Keithley 6517A electrometer. A PTW30013 Farmer chamber is used for specific tests (described below). The chamber center is placed 7 cm downstream from the third collimator. The radiation beam covers the 2.5 cm active length of the chamber to avoid partial-volume irradiation uncertainties. The chamber is mounted on a motorized linear translator perpendicular to the beam axis to allow for profile scans as well as on-axis transmission measurements. The radiation beam enters the chamber from its side because head-on irradiation used in some previous studies[2,19–22] introduces unnecessary radiation-induced cable leakage and makes the Monte Carlo-calculated transmission data more sensitive to the chamber details (particularly the stem).

The two main buildup caps used with the Farmer chambers are made of, respectively, polymethylmethacrylate (PMMA) and a W-alloy (90% W, 5% Ni, and 5% Cu). A third pure Al cap is used for specific tests (described below). The caps have wall thicknesses roughly equal to the CSDA range of 10 MeV electrons in their respective materials. The same caps are used for all MV beams to reduce the number of variables in the experiment. For a given MV beam and a given attenuator, the attenuator lengths used with the W-alloy cap are the multiples 2, 4, 6, 8, and 10 of the smallest length, while the multiples 1, 3, 5, 7, and 9 are used with the PMMA (or Al) cap.

The setup is aligned to a laser beam. Overall, the setup dimensions and the alignment are known with sub-mm accuracy. Temperature is recorded at the locations of the monitor and Farmer chambers to ensure that there is no differential temperature effect between the two locations (e.g., due to heat convection from the target). Pressure and humidity are also monitored. The experiment is automated and computer controlled using NRC software, including the movement of the attenuator rack and the data acquisition from the three chambers (monitor, field, and Farmer) and from other sensors. Each component is individually commissioned at the beginning of the experiment. The automated measurements are monitored with a CCTV system.

II.C. Data acquisition and experimental corrections

II.C.1. Equilibration

Irradiation during the initial daily setup reduces linac warmup effects and Farmer chamber settling effects.[23] Settling/warmup effects for the electrometers are avoided by keeping them always ON and biased.

II.C.2. Steering

The extended dimensions of the setup and the high degree of collimation amplify small steering issues. Therefore, a PTW Starcheck 2D ion-chamber array (3 mm resolution) with a 2.5-cm-thick PMMA buildup plate is periodically placed in front of the third collimator to check the steering. If necessary, the beam is manually steered until its peak aligns with the laser, with more emphasis on horizontal steering in the direction of the chamber diameter. Farmer chamber scans behind the third collimator are used to confirm profile symmetry, typically within 0.3 mm (resteering if necessary). Figure 2 shows an example of the measured beam profiles.

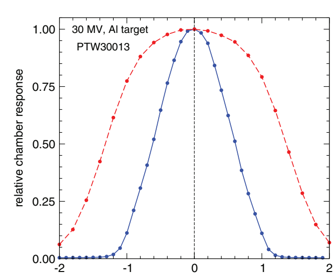

FIG. 2. Horizontal beam profiles in the absence of an attenuator. Solid line: past the first two collimators at the location of the upstream surface of the attenuator (95.1 cm from the linac exit window). Dashed line: past the third collimator at the location of acquisition of the transmission signal (298.8 cm from the linac exit window). The profiles for other MV beams and targets are similar.

II.C.3. Typical measurement protocol and parameters

Measurements are made with the four possible attenuator/buildup-cap combinations (C/W-alloy, C/PMMA, Pb/W-alloy, and Pb/PMMA). The five attenuator lengths for a given attenuator/cap combination are placed on the translation system in random order to reduce bias from slow drifts in the direction of the beam. One data point is acquired per attenuator length, plus one data point with no attenuator and one with the Cu rod for a total of seven points. The process is repeated for the whole rack 4–8 times to characterize short-term repeatability. This sequence (as opposed to successive data acquisition for each attenuator length before moving to the next) further reduces bias from beam drifts. Measurements are repeated with the Farmer chamber polarity reversed. To characterize long-term repeatability, measurements for different beams and targets were repeated intermittently over 15 months. The 15 MV beam has the largest number of long-term repeats (up to five long-term repeats per target per polarity over a year). Several of the sets measured with the PMMA cap are repeated with the Al cap, and a few of the sets measured with the A19 chamber are repeated with the PTW30013 chamber. These additional data are used to test the relative detector response calculations with EGSnrc, and they are used later[6] to test the detector-independence of the unfolded photon spectra.

Charge integration times varied from 5 s for the air signal to 60 s for the signal with the longest attenuators, leading to data acquisition time of $\leq$30 min per attenuator rack per polarity. The chosen integration times are short enough to allow for short-term beam instabilities to be identified by the field-to-monitor ratio and eliminated (instead of being averaged out with increased signal fluctuations). Linearity of the signal with integration time was established. The uncertainty component for repeatability is not reduced with further increase in integration times.

The monitor chamber currents are $\sim$5 to 20 nA going from 10 to 30 MV, while the field chamber currents are $\sim$50 times smaller. The Farmer chamber currents with the W-alloy cap and with no attenuator present are $\sim$50 to 250 pA going from 10 to 30 MV. These currents correspond to a dose rate to water of $\sim$15 to 80 cGy/min if the bare chamber were in a water phantom. With the longest attenuators, the Farmer chamber currents are $\sim$60 times lower than the currents with no attenuators. When the PMMA cap is used, the currents are roughly 60% of those with the W-alloy cap. Attempts to increase the beam currents for lower MV beams to offset the lower bremsstrahlung yield were limited by poorer beam control and excessive target heating.

II.C.4. Data normalization and drift corrections

For a given attenuator rack, the temporal variation of the field-to-monitor chamber ratio exhibits one of the following four patterns. (a) A sharp change in the ratio, indicating a large temporary drift in the direction of the beam. The data during this unstable period are excluded during averaging. An example is shown by the solid line in Fig. 3(a), where

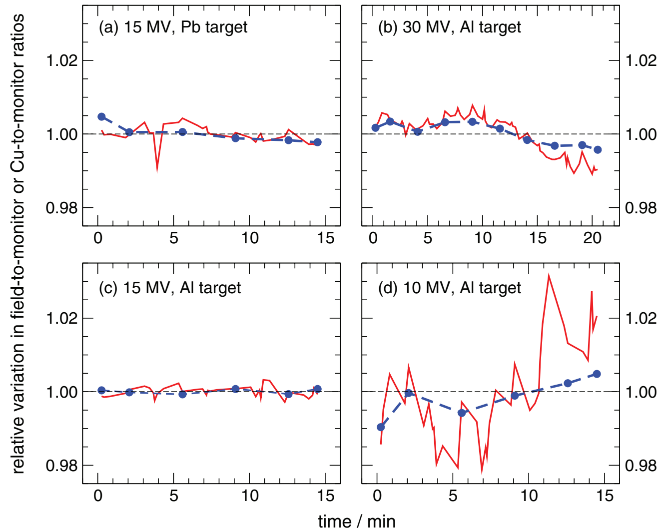

FIG. 3. The use of the field-to-monitor ratio (solid lines with no symbols) and the Cu-to-monitor ratio (dashed lines with filled circles) in various situations to monitor and correct for linac beam instabilities. The scales of the ordinates in all panels are the same to make clear the differences in the four temporal patterns. See Sec. II.C.4 for details.

a sudden 1% drop in the ratio is seen around minute 4. This emphasizes the importance of reasonably short charge integration times, as discussed above. No universal threshold for data rejection is applied because the threshold depends on the overall temporal behavior of the field-to-monitor ratio for a given beam at a given time period. (b) A mostly smooth change in the ratio, which indicates a slow drift in the direction of the beam that affects the field chamber signal but is not recognized by the monitor chamber due to its large sensitive volume. In this case, the Cu-to-monitor ratio is used to correct the Farmer-to-monitor signal for these second-order drifts, with linear interpolation in time between the sparse Cu-to-monitor data. An example is shown in Fig. 3(b), where the Cu-to-monitor ratio exhibits a temporal pattern similar to the field-to-monitor ratio, indicating that the Cu-to-monitor ratio can reliably correct for the drift. As Fig. 3 shows, the field-to-monitor ratio is too noisy to be used for the drift correction, and it is only used for qualitative analysis and data rejection. (c) Small random changes in the field-to-monitor ratio, which is the ideal situation since it indicates negligible beam drifts—e.g., the $\pm$0.25% in Fig. 3(c). In such a case the Cu-to-monitor correction is neither useful nor needed. (d) A slow change in the field-to-monitor ratio superposed on large fluctuations [Fig. 3(d)]. In this case, the correction using the Cu-to-monitor signal accounts for part of the drift, and the rest of the fluctuations increase the measurement uncertainty. Overall, the magnitude of the correction for beam drifts using the Cu-to-monitor ratio is $\leq$2%.

For the 10 MV beam, transmission signals are twice as noisy as other beams. The noise is largely independent of the signal size (unlike other beams where the noise is larger for smaller signals. Also, the variations in the field-to-monitor ratio are larger and less smooth [e.g., Fig. 3(d)]. This indicates beam instability issues, rather than signal-to-noise issues, and thus cannot be addressed by increasing the beam current or the charge integration times.

II.C.5. Leakage

Leakage is the signal in the absence of the radiation beam for the combined system of the Farmer chamber + extension cable + electrometer. In an initial setup, leakage from a 50 m cable made ~50% of the total leakage (1.3% for the smallest signals). Therefore, the electrometer was moved inside the linac room, shielded, and connected to the chamber using a short cable to reduce the leakage to sub-fA ±1 fA. The improved uncertainty on transmission signals due to leakage is ≤0.3%. Leakage is found to not be affected by turning ON or OFF the RF systems (with the radiation beam absent in both cases).

II.C.6. Polarity effects

It is difficult to identify the sources of the polarity effects. Strictly speaking, the polarity correction in this study, P_{pol}, is an "apparent relative" correction: "apparent" because it is assumed to include all extracameral effects and radiation-induced leakage, and "relative" because it is determined for the Farmer chamber signals after normalization to the respective monitor signals and after the drift correction by the Cu-to-monitor ratio. The assumption made is that the causes of polarity cancel out when the absolute signals with the two opposite polarities are averaged. For all transmission data in this study, measurements are made at both polarities for the Farmer chamber (±300 V). A five-minute waiting period is applied after polarity reversal to ensure that the chamber reached its equilibrium, because polarity cycling induces the worst settling behavior.[23] The good shielding in front of the stem of the Farmer chamber suggests that most of the correction is due to cable effects, rather than stem effects.

Figure 4 shows examples of the measured P_{pol}, defined as in the AAPM TG51 protocol,[24] with the negative signal as the reference. The following observations can be made based on the full P_{pol} data (not only those in Fig. 4). The value of P_{pol} is typically unity within 2.5%, but it can be as large as 6% for the smallest signals. The increase in P_{pol} as the transmission signal decreases is because the extracameral effects are independent of the main signal size, and thus make a larger fraction of the smaller signals. Figure 4(a) shows that repeat measurements at different times give different P_{pol} values, which is due to minor changes in the setup such as cable positions and shielding details. However, the polarity-corrected signals (before normalization to the air signal) agree with each other to ~0.15% (above the typical uncertainty from repeatability). This can be taken as confirmation of the accuracy of the applied polarity correction. The air signals with no attenuator (i.e., a transmission of unity) are the closest to typical clinical dose rates. For these signals, P_{pol} values are consistent with TG51 recommendations[24] (i.e., unity within 0.3%), and they do not exhibit clear MV-dependence, in accord with previous studies.[16,25] For the P_{pol} values versus transmission, no conclusive evidence of MV-dependence is found, although

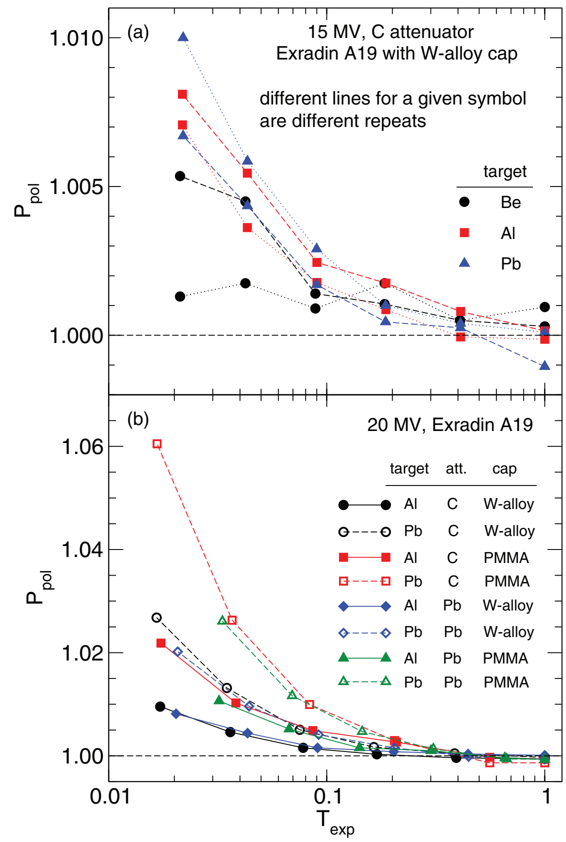

FIG. 4. The polarity correction factor, P_{pol}, versus the experimental transmission signals, T_{exp}. See the text for statements based on the full P_{pol} data (rather than only the data shown).

Fig. 4(a) versus Fig. 4(b) seemingly suggests otherwise. For some beams [e.g., the 20 MV beam in Fig. 4(b)], P_{pol} depends on the bremsstrahlung target material. However, no clear mechanism is found to explain such clear target dependence, particularly that it is not the case for all MV beams. The value of P_{pol} is larger for the PMMA cap compared with the W-alloy cap [e.g., Fig. 4(b)], which could be caused by the smaller signal with the PMMA cap and/or by more scatter from the cap into the cables. There is only a very subtle increase in P_{pol} for the C attenuators compared with the Pb [e.g., Fig. 4(b)]. For the PTW30013 chamber, the magnitude of P_{pol} values and their variation with transmission are different from those for the A19 chamber (not shown). The observations above collectively underline that the polarity correction is non-negligible and that it is sensitive to minor detector and setup details and should thus always be measured for the exact setup used.

II.C.7. Ion recombination

P_{ion} is investigated because charge collection efficiency varies with dose rate, which changes by a factor of ~60 in a transmission curve. The correction is determined using the approach of McEwen.[16] The correction for the most extreme case (30 MV beam and a W-alloy cap) varies from 0.18% to 0.07% going from the largest to the smallest transmission signals. Therefore, the maximum differential effect of ion recombination is only 0.11%.

II.C.8. Room scatter

Room scatter is the corrected Farmer chamber signal when the radiation beam is ON but completely blocked. Unlike the polarity effect, room scatter contributes to the cavity ionization, rather than to the cable signal. It is experimentally determined using the shadow-cone technique whereby a 40-cm-long Pb rod is placed at 95.1 cm from the exit window to attenuate the photon beam by many orders of magnitude, and the Farmer chamber signal is acquired at the far end. Measurements are made for different MV beams at both polarities and with the A19 and the PTW30013 chambers. The signals are corrected by P_{pol} and P_{ion}. Room scatter is found to be 0.8% of the smallest signal for the 30 MV beam, and much smaller for lower MV beams. Its magnitude is largely chamber-independent.

II.C.9. Apparatus scatter

The effect of the apparatus components that are not part of the Monte Carlo model is investigated here. These components are the side attenuators, the table holding the setup, and the Al support rack. For side attenuators, comparisons of the measured signals for a given bar with and without various side attenuator configurations show that their contribution is negligible. Also, the permanent Cu rod experiences different side attenuators in different racks, and its signal remains constant within repeatability. For table scatter, the effect is investigated for different MV beams and attenuators by adding a large aluminum plate on top of the attenuator rack to mirror the table effect, and no signal increase is observed. For the Al support rack, transmission signals measured with and without the rack are the same within repeatability. EGSnrc sensitivity studies indicate that the combined scatter from the three components is $\leq$0.01% of the smallest transmission values.

II.C.10. Lower transmission cutoff

When data are acquired for transmission signals $\leq$1% by using a sixth, longer attenuator, both the magnitude and the uncertainty of the corrections above significantly increase. Therefore, those extra points are not included in the analysis.

II.C.11. Data processing

Based on the details above, the following sequence of processing the raw signals is individually applied for each MV/target/attenuator/detector combination. (a) The data acquired during short-term beam instabilities are identified and excluded. (b) The Farmer signals are normalized to their respective monitor chamber signals. (c) Drift corrections are applied using the Cu-to-monitor ratio. (d) Short-term repeats for a given polarity are averaged for the drift-corrected signals. (e) Polarity and ion recombination corrections are applied. (f) The corrected room scatter signal is subtracted from the corrected Farmer chamber signals. (g) Long-term repeats of the corrected Farmer chamber signals are averaged. (h) The averaged data are normalized to the air signal to obtain a fully corrected transmission curve.

II.D. Experimental uncertainty budget and influence quantities

The experimental uncertainty budget, derived according to The ISO Guide on Uncertainty in Measurement,[26] is given in Table II.

II.D.1. Short-term beam drifts, P_{pol} and leakage

The conservative approach adopted is to assume that the three components are not correlated and can be added in quadrature. The first two components are evaluated by calculating the statistical uncertainty of short-term repeats for polarity-corrected signals, then assuming that $\frac{1}{\sqrt{2}}$ of that uncertainty is due to beam drifts that have not been fully accounted for, and the other $\frac{1}{\sqrt{2}}$ is due to the uncertainty on the polarity correction. For instance, for the 10 MV beam and the smallest signals, the uncertainty for short-term repeats is 0.35%, therefore an uncertainty of $0.35/\sqrt{2} = 0.25\%$ is assigned to both short-term beam drifts and polarity, as seen in Table II. For the 10 MV beam, the drift and polarity uncertainties are roughly twice those for other beams, and they are less dependent on the signal size. This is reflective of the beam instability issues discussed earlier for that beam.

II.D.2. Long-term repeatability

This component characterizes the stability of the electron beam energy, and it indicates changes on in addition to the short-term ones. The air-to-Cu signal was monitored for the 15 MV beam for a year and was found to be constant within 0.1%. This is a confirmation that the incident electron energy has not changed, and it is another important use of the Cu signal. The klystron had to be replaced during the course of the measurements, and excellent long-term repeatability was still achieved, which provides confidence in the values assigned to this component. For the 10 MV beam, the value for this component is obtained through detailed stability investigation of the largest signal, which indicates that the standard deviation of a series of means is 0.2% larger than the standard uncertainty on the full data.

II.D.3. Attenuator mass thickness

For C, when transmission data are acquired for different bar combinations that add up to the same physical length, variations of up to 1.2% are observed. When EGSnrc calculations for these bar combinations are performed using their individual mass thicknesses, the relative variations in the EGSnrc-calculated transmission data exquisitely matched the experimental observations within 0.1% above repeatability. This indicates that the individual mass thicknesses should be used in the Monte Carlo calculations. The 0.1% level of agreement just mentioned is taken as the uncertainty component from mass thickness variations that are unaccounted for. For Pb, the uncertainty comes from using the average density due to minor irregularities in the rods.

TABLE II. The uncertainty budget for the experimental transmission data, T_{exp}. Values are given for one relative standard uncertainty, u. Some components are beam-specific, thus the components for the 10 MV beam are presented separately. The leakage component is estimated by statistical means (Type A), while all others are estimated by nonstatistical means (Type B). For the corrections listed, the u values are not the magnitudes of these corrections but rather the uncertainties on T_{exp} caused by the uncertainties on these applied corrections. The total uncertainty is obtained by adding its components in quadrature.

	u (%) for T_{exp}: ∼1 → ∼0.017			
	10 MV		15, 20 and 30 MV	
Uncertainty component	C attenuator	Pb attenuator	C attenuator	Pb attenuator
Linac and detection system				
Short-term beam drifts	0.2 → 0.25	0.2 → 0.25	0.07 → 0.15	0.07 → 0.15
P_{pol}	0.2 → 0.25	0.2 → 0.25	0.07 → 0.15	0.07 → 0.15
Leakage	0.003 → 0.3	0.003 → 0.3	0.001 → 0.1	0.001 → 0.1
Long-term repeatability	0.2 → 0.2	0.2 → 0.2	0.1 → 0.15	0.1 → 0.15
P_{ion} (Ref. 16)	0.03	0.03	0.03	0.03
Monitor chamber stability[a]	0.1	0.1	0.1	0.1
Electrometer nonlinearity	0.05	0.05	0.05	0.05
Attenuators				
Mass thickness	0.1	0.15	0.1	0.15
Density nonuniformity	0.1	0.0	0.1	0.0
Impurities	0.05	0.02	0.05	0.02
Incident electron beam				
Mean energy	0.15 → 0.67	∼0.05	0.1 → 0.5	0.01 → 0.2
Radial spread	0.15	0.15	0.15	0.15
Divergence	0.1	0.1	0.1	0.1
Total uncertainty				
Without u of the electron beam	0.41 → 0.55	0.41 → 0.55	0.26 → 0.35	0.26 → 0.35
With u of the electron beam	0.47 → 0.88	0.45 → 0.58	0.33 → 0.64	0.31 → 0.44

[a]The corresponding component for the Farmer chamber is negligible (Ref. 16).

II.D.4. Attenuator density nonuniformity

For C, its manufacturing method (isomolding) and its very fine grain size (10 μm) suggest excellent density uniformity. CT scans of the bars did not indicate any bores or patterns, and suggested a 0.5% estimate of density nonuniformity. A better estimate using the CT data was precluded by the imaging and reconstruction artefacts. To supplement the CT results, transmission measurements for a few bars are compared with and without the bars rotated in the orthogonal and longitudinal directions. This allows the radiation beam cone to sample different portions of the bars. Variations at the 0.1% level above repeatability are observed, which is taken as the uncertainty component for density nonuniformity. For Pb, this component is negligible.

II.D.5. Attenuator impurities

The effect of reasonable variations in impurities is calculated deterministically[1] using point-source spectra of different MV beams. The uncertainty is larger for C attenuators than it is for Pb because the ash content is "assumed" rather than "supplied."

II.D.6. Incident electron beam parameters

The uncertainty components from the incident electron beam are investigated because this study is a primary benchmark. The total uncertainty is given without and with these components because they are not known for typical clinical beams and thus would not be part of an uncertainty budget of transmission measurements on a typical clinical linac. For the mean energy, EGSnrc calculations are performed with mean energies both at the actual bending magnet values and at values one standard deviation (0.4%) larger. The effect on the calculated transmission values is much larger with the C attenuators than it is with Pb (the reason is discussed in Sec. III.A), and it is the largest component in the uncertainty budget for C. The uncertainty component from the focal spot size is estimated from the difference in EGSnrc calculations when the FWHM of the radial spread is changed from 1 to 2 mm (both values are noted in Ref. 11).

II.D.7. Positioning and alignment

To investigate the uncertainty component related to positioning, transmission signals are measured with C and Pb attenuators shifted laterally continuously in sub-mm intervals. Given the lateral dimensions and the physical extent of the attenuators of both materials, experimental transmission signals did not change for shifts up to 5 and 2 mm for C and Pb, respectively. Offsetting the Farmer chamber position in the vertical direction within ±1.5 mm did not show any differential effect, both experimentally and in EGSnrc simulations. Therefore, attenuator and detector positioning uncertainties are assumed negligible. For the uncertainty component due to misalignment, transmission measurements after repeated reinstallation of the three collimators show that this component is negligible.

II.D.8. Other influence quantities

(a) The potential charge storage[27] in the large insulating PMMA cap is investigated experimentally by comparing repeats at the end of a day or a week of heavy irradiation against those with fresh irradiation. The effect is found to be negligible. (b) Since the two buildup caps used have different physical dimensions, the difference in the spectra seen by the two caps is investigated using EGSnrc and found to be negligible. (c) Since the clinically useful primary spectrum is the one at the machine isocenter rather than the one at the chamber location at ∼3 m, the primary photons at the isocenter that do not reach the detector because of their larger divergence angle are investigated using EGSnrc and their effect on the spectrum is found to be negligible.

II.E. Monte Carlo modeling

BEAMnrc (Refs. 28 and 29) is used to model the measurement setup from the linac exit window to the downstream end of the third collimator. Target dimensions are those from Table I. The incident electron parameters are those from Sec. II.A. Based on the discussions in Secs. II.B and II.D.3, the individual mass thicknesses of the C attenuators are used, while the average density and the physical lengths of the Pb attenuators are used. The attenuator impurities listed in Sec II.B are included. The monitor chamber is modeled from its blueprints. BEAMnrc simulation efficiency is improved using directional bremsstrahlung splitting (DBS) (Ref. 30) with a splitting field diameter of 6 cm at the bottom of the third collimator. Using a smaller splitting field makes "fat" particles play a significant role, and eliminating them leads to errors up to 0.8% in the calculated transmission values. In addition to DBS, photons are split at the upstream face of the attenuator. As the attenuator length increases, the splitting number is increased exponentially to compensate for the exponential signal reduction. This additional splitting reduces the disparity in simulation efficiency over the factor of ∼60 signal change.

The usercode cavity (Ref. 31) is used to model the Farmer chambers (Exradin A19 and PTW30013) from their blueprints.[32] BEAMnrc is used as a shared library input to cavity to eliminate the need for phase-space storage and for particle recycling. This means that the detector energy response is folded into the calculated transmission data. Doses to the cavity of the chamber are calculated to ∼0.15% statistical uncertainty.

The most-accurate low- and high-energy physics options available in EGSnrc are used in all simulations. This has to be done because the extended dimensions (∼3 m), the extreme attenuation, and the extreme collimation strongly amplify what would otherwise be small physics effects. For instance, Rayleigh scattering is commonly known to be relevant only for low energies. However, our EGSnrc simulations for 10 MV (the lowest MV, with 1.5 MeV mean photon energy) show that ignoring Rayleigh scattering with Pb attenuators leads to errors up to 2% in the smallest transmission data. Other second-order effects that are turned ON are incoherent scattering corrections (binding effects, radiative corrections, and double Compton), electron–electron bremsstrahlung in the target,[33] electron impact ionization,[34] and explicit triplet (i.e., incoherent pair) production. The photon energy cutoff is 10 keV. For our transmission analysis studies, we implemented into EGSnrc a fine-resolution version of the NIST XCOM photon cross sections, and this version is used throughout this study.

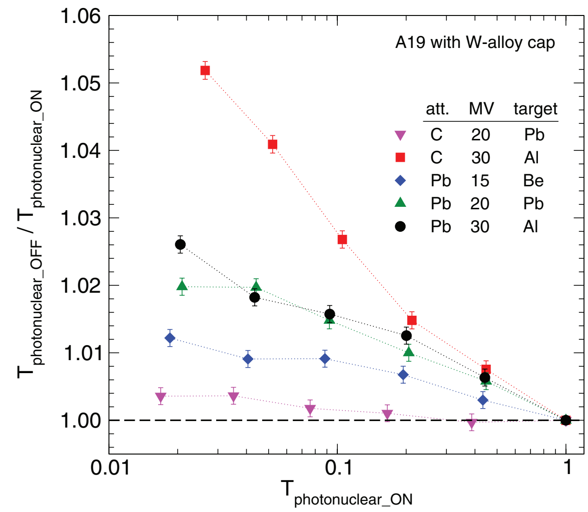

FIG. 5. The errors introduced in the calculated transmission data, T, if the photonuclear effect is ignored only in the attenuators. Transmission data with and without photonuclear attenuation are both calculated using EGSnrc. The effect is up to 5.2% for $T \geq 1.7\%$. For the attenuators and energies in this study, the photonuclear effect is relevant for C between ∼17 and 30 MeV and for Pb between ∼8 and ∼25 MeV.

Photonuclear cross sections have a resonance from a few MeV to tens of MeV (depending on the isotope), and they contribute a few percent to the total photon cross sections.[35] Recently, EGSnrc has been upgraded[36] for our transmission analysis studies to model photonuclear attenuation (without modeling secondary particles). In the current study, EGSnrc calculations have photonuclear attenuation ON everywhere except in the chamber. Figure 5 shows that ignoring the photonuclear effect only in the attenuators leads to errors in the calculated transmission data of up to 5.2%. In addition, photonuclear cross sections vary strongly with energy for the Be, Al, and Pb targets and for other materials in the path of the photon beam. Ignoring the photonuclear effect in the target and other materials leads to small spectral differences at the detector location, which leads to additional errors up to 0.4% in the EGSnrc-calculated transmission data. Therefore, for the photon beams of this study, the total photonuclear effect is ≤5.6% for transmission values ≥1.7%, and it would be larger for smaller transmission values.

The EGSnrc-calculated transmission data are found to be particularly sensitive to the choice of the bremsstrahlung angular sampling option. EGSnrc offers two sampling options: KM and Simple. The KM option is a modification of the 2BS formula from Koch and Motz.[37] It offers a compromise

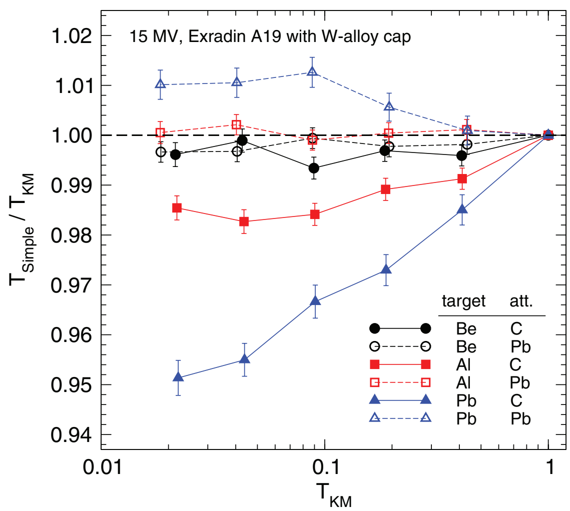

FIG. 6. The effect of using the different bremsstrahlung angular sampling options offered in EGSnrc (KM and Simple) on the calculated transmission, T. The 15 MV beam is typical of others.

between relaxing the extreme-relativistic and the small-angle approximations on one hand, and accounting for the nuclear screening effect on the other hand. The Simple option uses only the leading term of the KM option for faster sampling. The Simple option is more widely used than the KM option because it leads to large gains in simulation efficiency with DBS.[30] It is not immediately obvious which of the two options is more accurate because the underlying assumptions are not strictly satisfied for either of them. Figure 6 shows the effect of the angular sampling options on the calculated transmission. The effect is because after sampling the energy of a bremsstrahlung photon, the different energy-angle formulae that are used to sample the emission angle lead to slightly different spectra seen by the Farmer chamber due to the high degree of collimation. The effect generally increases with the atomic number of the target and can be up to 5%. For a given mass thickness, the effect depends on the material of the attenuator (e.g., C compared with Pb). The variation of the effect with beam energy is small (not shown). An important observation is that the absolute cavity doses (i.e., before normalization to the cavity dose with no attenuator) when using the two sampling options differ by up to 16%, 9%, and 4% for the Be, Al, and Pb targets, respectively. A related observation is that in the previous NaI measurements of photon spectra on the same linac, the absolute EGSnrc yield calculations[38] on the beam axis using the KM option were within the 5% experimental uncertainties of the NaI measurements (Figs. 5 and 6 in Ref. 38). Combining these two observations, it can be concluded that for on-axis yields the KM option is more accurate. Therefore, the KM option is used throughout this study. This worsens the simulation efficiency by up to a factor of 2.6—although if there were a flattening filter it would worsen the efficiency significantly more. A typical calculation, not optimized for efficiency, takes of the order of a few tens of hours on a single 3.6 GHz CPU core. Finally, it is difficult to use only the comparison between the measured and calculated transmission data of this study to draw a conclusion regarding the accuracy of the KM and Simple options. This is because cross section uncertainties are amplified by the strong attenuation in a transmission curve, which complicates the analysis.

TABLE III. Same as Table II but for the EGSnrc-calculated transmission data, T_{EGSnrc}. The Monte Carlo statistical uncertainty is Type A and the other components are Type B.

Uncertainty component	u (%)
Statistical uncertainty	0.15
Detector energy response	0.15
EGSnrc (Fano test) (Ref. 44)	0.1
W/e variation with energy	0.1
Bremsstrahlung energy-angle distributions	Not included
Cross sections	Not included
Total	0.25

The uncertainty budget for the EGSnrc-calculated transmission data is given in Table III. The uncertainty from the detector energy response (which is folded into the calculated transmission data) is deduced from the level of agreement between measurements and EGSnrc calculations for the relative Farmer chamber response (Sec. III.A). The upper bound estimate on the variation of W/e from ^{60}Co to 25 MV is 0.25% (68% confidence).[39] Applying this to the range of spectral variation versus transmission gives an uncertainty of ∼0.1%. From the large effects shown above when using different bremsstrahlung angular sampling options, it can be extrapolated that the accuracy of even the more accurate energy-angle distribution will have an effect on the calculated transmission data, but this is beyond the scope of this study. Geometric uncertainties are considered part of the experimental uncertainty budget (Sec. II.D), and they are not included in the Monte Carlo budget to avoid double counting.

III. RESULTS AND DISCUSSION

III.A. Sensitivity of transmission data (relative comparisons)

Figure 7 shows comparisons between measurements and EGSnrc calculations of the sensitivity of transmission data to a number of small changes in the experimental setup and in the operating parameters. The uncertainty on a given ratio is smaller than that on its components because many correlated Type B uncertainties (e.g., those due to cross sections) cancel out. Overall, excellent agreement between measurements and calculations is obtained. The data suggest that, on average, EGSnrc is accurate for relative ion chamber response calculations at the 0.2% level. This supplements previous experimental validations at low energies[40,41] and at high energies.[42]

In Fig. 7(a), the large variation (∼13%) in transmission for a relatively small change in the atomic number of the buildup cap material underlines the importance of accurate detector response modeling in transmission analysis to avoid significant errors in the unfolded spectra.[1] The agreement in Fig. 7(a) for the relative effect of the buildup cap is an indirect validation of the EGSnrc-calculated detector energy response with these caps.[1] The level of agreement in Fig. 7(a)

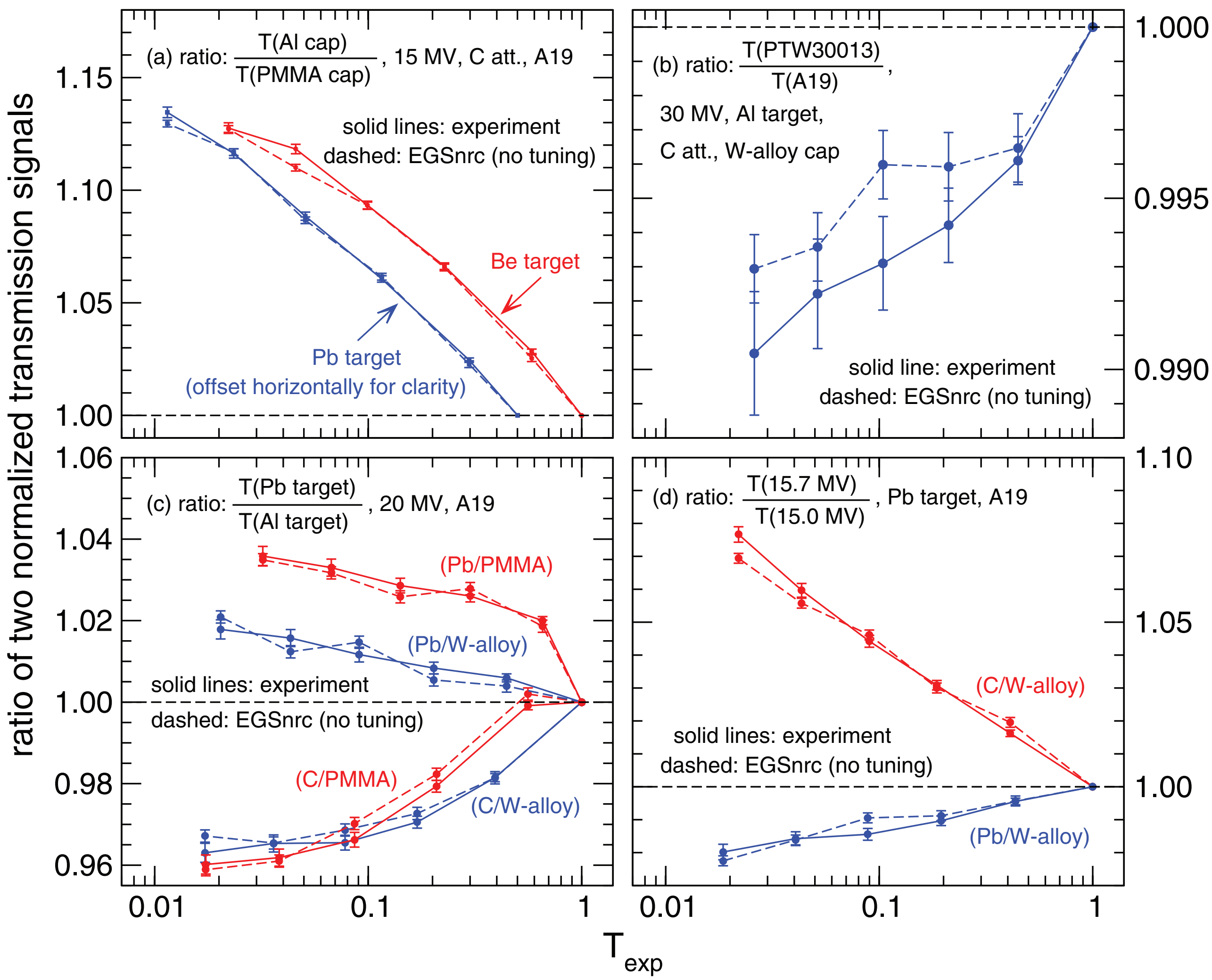

FIG. 7. Measurements and EGSnrc calculations of the sensitivity of transmission data to small changes in: (a) the material of the buildup cap, (b) the Farmer chamber construction details, (c) the bremsstrahlung target, and (d) the incident electron energy. The abscissae are the experimental transmission data, T_{exp}, from the denominator of the ratio plotted in each panel. In panels (c) and (d), the pairs shown are different (attenuator/cap) combinations. Note the very different scales of the ordinates.

is used to deduce an uncertainty component in Table III for the detector energy response.

Figure 7(b) shows that even for similar Farmer-class 0.6 cc chambers and the same buildup cap, transmission data are sensitive to the detector construction details, which indicates the importance of modeling such details. Given that the range of variation of transmission in Fig. 7(b) is only 1%, the ability of EGSnrc calculations to accurately model that change is remarkable.

Figure 7(c) demonstrates the sensitivity to the target material and the ability of EGSnrc to model it. The behavior is case-specific because of the interplay between the spectral shapes from the different targets, the detector energy response with different caps, and the energy dependence of the attenuation coefficient for different attenuators. For instance, the same four curves but for the 15 MV beam are all above unity.

Figure 7(d) shows that a 4.7% change in the incident electron energy leads to a ∼7% change in transmission for C attenuators. This is consistent with the uncertainty budget, where a ∼0.5% change is observed for a 0.4% change in the electron energy. The smaller effect with Pb attenuators (∼2%) should not be misinterpreted as lack of energy sensitivity. Rather, it is because the Pb attenuation coefficient has a minimum at ∼2.5 MeV. Therefore, even though the transmission values do not change significantly with energy, the contribution to them from photons at different energies does. The overall sensitivity to small energy changes is useful for accurate spectral unfolding.[6]

III.B. Direct comparisons of transmission data

Direct comparisons between the measured and the calculated transmission data are shown in Fig. 8. Unlike the relative comparisons of Fig. 7, the comparisons here are affected by all the experimental and the Monte Carlo uncertainty components, in addition to cross section uncertainties. The overall agreement is excellent for a reduction in transmission by a factor of ∼60, particularly that there is no tuning in the EGSnrc model. For C attenuators, the agreement is better than 2% for all beams except for the 10 MV beam, which is

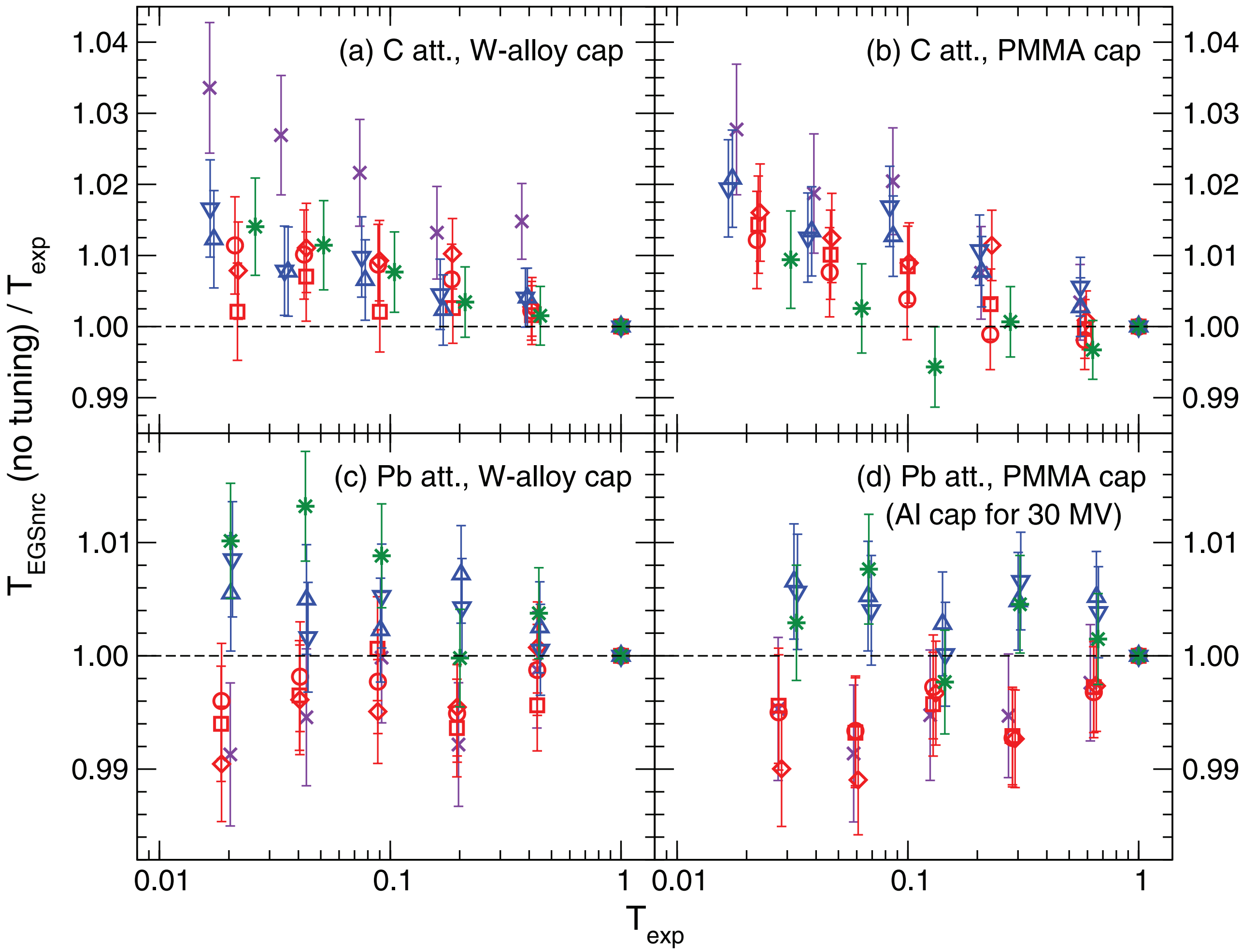

FIG. 8. Ratio of the transmission data calculated from a full EGSnrc model of the experiment, T_{EGSnrc}, to those measured experimentally, T_{exp}. Each panel includes data for the following MV/bremsstrahlung-target combinations: 10 MV/Al (×), 15 MV/Be (○), 15 MV/Al (□), 15 MV/Pb (◊), 20 MV/Al (△), 20 MV/Pb (▽), and 30 MV/Al (∗). The 1σ uncertainty bars are obtained by adding in quadrature the totals of the uncertainty budgets for T_{exp} (Table II, including the components due to electron beam uncertainties) and T_{EGSnrc} (Table III). Photon cross section uncertainties are not included.

better than 3.4%. For Pb attenuators, the agreement is typically better than 1%.

For the photon energies relevant to the current study, Hubbell[43] gave a rough "envelope of uncertainty" of 1%–2 % on photon cross sections (not including the effect of ignoring the photonuclear component). For the current study, uniformly scaling the XCOM photon cross sections used in the EGSnrc calculations by values within ±0.4% of unity makes the majority of the data in Fig. 8 agree with unity within the uncertainty bars. Based on this observation and the level of detail presented earlier for both the experimental and the Monte Carlo aspects, it is plausible to attribute the discrepancies beyond the uncertainty bars in Fig. 8 to cross section uncertainties.

Although cross section uncertainties alone are enough to explain the small discrepancies in Fig. 8, other possible explanations are explored here, but they are extremely difficult to verify because cross-section induced errors are not known accurately. Figure 8 shows that the agreement worsens for smaller transmission values, which is obvious for C and more subtle for Pb. This trend is characteristic of a cross section effect, but can also be due to other effects that make a larger fraction of smaller transmission values (similar to the effects of P_{pol} or the attenuator mass thickness that are already accounted for). For C attenuators, EGSnrc results are always larger than experiment, which is reassuring that it is unlikely to be due to additional scatter effects that are unaccounted for (because they would have made the experimental results larger than the EGSnrc results). The agreement for the 10 MV beam is clearly worse than that for other beams. This is reflective of the beam instability (and possibly other) issues for that beam. There are subtle hints of MV-clustering of the data in Fig. 8, which may indicate second-order beam-specific issues (related to the linac performance) that have not been accounted for experimentally. It might also indicate a small energy dependence of cross section errors.

III.C. Suggestions for accurate transmission measurements

The experimental protocol developed in this study allows for transmission measurements to be made with ∼0.4% uncertainty (not including electron beam uncertainties) over a signal change of a factor of ∼60. Based on the details presented earlier, the following suggestions can be made for accurate experimental measurements down to transmission values of ~1.7%. Reference class 0.6 cc Farmer chambers present a reasonable compromise between reliability, signal size, and narrow-beam geometry. Their response can be easily manipulated with the choice of the buildup cap material. Equilibration at the start of the irradiation and when reversing the polarity is important.[23] Alignment and beam drifts should be closely checked at the detector location because the narrow-beam geometry amplifies their effects. Reliable corrections for linac output fluctuations and for beam drifts can be achieved with the combined use of the monitor signal, the field-to-monitor ratio, and the Cu-to-monitor ratio. A reasonable number of randomized short- and medium-term repeats is necessary to reduce bias from slow beam drifts. Reasonably short signal collection times help identify and eliminate the data acquired during short-term beam instabilities. Automating the measurements has its obvious conveniences, but it also facilitates more randomized repeats and improves beam stability because of the reduced beam interruption. Polarity corrections are large and variable, therefore they should be measured individually for each data set; simple precautions such as irradiating the chamber side-on (not head-on) or adjusting cable positions help reduce the magnitude and the uncertainty on polarity correction. Ion recombination is not a major correction for the typical dose rate variations in transmission measurements. Leakage varies significantly depending on the chamber-cable-electrometer system used, therefore the contribution of leakage should be characterized for the individual system components, and reduced if necessary (e.g., larger chamber, shorter cables, and/or different electrometer). If the electrometer has to be moved into the radiation room (as done in this study), it should be shielded to protect its radiation-sensitive circuitry without blocking proper heat exchange. Room scatter can be quantified using the shadow-cone technique. Apparatus scatter can be quantified experimentally and/or by Monte Carlo simulations. Accurate knowledge of the mass thickness of the attenuators is critical. The mass thickness can be determined accurately using a combination of linear dimensions, volume measurements, radiation measurements, CT scans, and Monte Carlo sensitivity studies. High-purity attenuators are not essential, but they reduce the uncertainty due to the inexact knowledge of the impurities. Temperature should be individually monitored at the different locations where signals are acquired, and corrected for if necessary. All the corrections above should remain at the level of small perturbations to the main transmission signals in order for the fully corrected signals to be credible. Monte Carlo simulations are a useful tool for systematic investigation of influence quantities to confirm and/or supplement experimental sensitivity studies.

The fully corrected transmission signals still include unavoidable components from nonprimary radiation: forward scatter (coherent or incoherent) in the attenuators, positron annihilation, scatter from and leakage through the collimators, attenuation and scatter in the intervening air, etc. For the purpose of benchmarking a Monte Carlo code, these effects do not need to be corrected for because they are included in both the measured and the calculated transmission data. However, if it is desired to correct for these effects to obtain a pure primary transmission signal (e.g., in the context of unfolding photon spectra from transmission data), the methods that were developed and validated earlier[1] to correct for nonideal attenuation conditions should be applied to the fully corrected experimental signals.

IV. CONCLUSIONS

In this study, detailed transmission measurements are performed and used to benchmark the `EGSnrc` system. The hybrid experimental/Monte Carlo nature of this study was a catalyst for refinements on both sides. On the experimental side, the dominant potential contributors to measurement uncertainties are beam drifts, polarity effects, leakage, and attenuator mass thickness. Ignoring the experimental influence quantities investigated in this study can collectively introduce errors of more than 10% in the measured transmission signals. On the Monte Carlo side, accurate `EGSnrc` calculations require the use of the most accurate data and physics models available in `EGSnrc` (including second-order effects). In particular, accurate calculations require using the `KM` option for bremsstrahlung angular sampling, which is shown to be more accurate than the `Simple` option. The newly added photonuclear attenuation has a significant effect on the calculated transmission values for higher MV beams. Relative transmission comparisons imply that `EGSnrc` is accurate within 0.2% for relative ion chamber response calculations over a wide range of spectral variations with transmission. Direct comparison of measured and calculated transmission data shows agreement better than 2% for C (3.4% for the 10 MV beam) and typically better than 1% for Pb. The differences can be explained by acceptable photon cross section changes of $\leq$0.4%. Given the small experimental and computational uncertainties in this study, it can be concluded that cross section uncertainties are the ultimate limiting factor for the accuracy of the calculated transmission data (Monte Carlo or analytical), and consequently the accuracy of any extracted spectral information. The lowest energy beam in this study is 10 MV (the lowest stable MV beam on the linac). However, the benchmark results can be extrapolated down to 6 MV since there are no large changes in the physics processes or the uncertainties on the cross section data. The beams in this study are flattening-filter free, but the methods and conclusions are equally applicable to beams with flattening filters. A supplemental web report[9] contains the data needed for others to benchmark Monte Carlo codes against the experimental and `EGSnrc` results.

ACKNOWLEDGMENTS

The authors thank Carl Ross of NRC for his invaluable assistance with the operation of the Vickers research linac and for many insightful discussions on different experimental aspects, Matt Bowcock of Carleton University for assistance with the attenuator assembly design, David Marchington of NRC and Philippe Gravelle of Carleton University for machine work, Dan La Russa of The Ottawa Hospital Cancer

Centre for the CT scans of the graphite bars, and Tong Xu of Carleton University for assistance with the analysis of the CT data. Elsayed Ali acknowledges the funding from a Vanier CGS. Dave Rogers acknowledges the funding from the CRC program, NSERC, CFI, and OIT.

[a)]Electronic mail: eali@physics.carleton.ca
[b)]Electronic mail: malcolm.mcewen@nrc-cnrc.gc.ca
[c)]Electronic mail: drogers@physics.carleton.ca

[1]E. S. M. Ali and D. W. O. Rogers, "An improved physics-based approach for unfolding megavoltage bremsstrahlung spectra using transmission analysis," Med. Phys. **39**, 1663–1675 (2012).

[2]P.-H. Huang, K. R. Kase, and B. E. Bjärngard, "Reconstruction of 4-MV bremsstrahlung spectra from measured transmission data," Med. Phys. **10**, 778–785 (1983).

[3]A. Catala, P. Francois, J. Bonnet, and C. Scouarnec, "Reconstruction of 12 MV bremsstrahlung spectra from measured transmission data by direct resolution of the numeric system AF = T," Med. Phys. **22**, 3–10 (1995).

[4]C. R. Baker and K. K. Peck, "Reconstruction of 6 MV photon spectra from measured transmission including maximum energy estimation," Phys. Med. Biol. **42**, 2041–2051 (1997).

[5]B. Armbruster, R. J. Hamilton, and A. K. Kuehl, "Spectrum reconstruction from dose measurements as a linear inverse problem," Phys. Med. Biol. **49**, 5087–5099 (2004).

[6]E. S. M. Ali, M. R. McEwen, and D. W. O. Rogers, "Unfolding linac photon spectra and incident electron energies from experimental transmission data, with direct independent validation," Med. Phys. (accepted).

[7]I. Kawrakow, "Accurate condensed history Monte Carlo simulation of electron transport. I. EGSnrc, the new EGS4 version," Med. Phys. **27**, 485–498 (2000).

[8]I. Kawrakow, E. Mainegra-Hing, D. W. O. Rogers, F. Tessier, and B. R. B. Walters, "The EGSnrc Code System: Monte Carlo simulation of electron and photon transport," NRC Technical Report PIRS-701 v4-2-3-2 (National Research Council Canada, Ottawa, Canada, 2011) (available URL: http://www.irs.inms.nrc.ca/inms/irs/EGSnrc/EGSnrc.html.

[9]E. S. M. Ali, M. R. McEwen, and D. W. O. Rogers, "Data for an accurate transmission measurement benchmark," Technical Report CLRP 12-02 (Carleton University, Ottawa, Canada, 2012), 15 pp. (available URL: http://www.physics.carleton.ca/clrp/transmission.

[10]M. S. MacPherson and C. K. Ross, "A magnetic spectrometer for electron energy calibration," Technical Report PIRS-0617 (59pp) (IRS, NRC, Ottawa, Canada, 1998), 59 pp. (available URL: http://irs.inms.nrc.ca/publications/reports/pdf/PIRS-0617-1998.pdf).

[11]C. K. Ross, M. R. McEwen, A. F. McDonald, C. D. Cojocaru, and B. A. Faddegon, "Measurement of multiple scattering of 13 and 20 MeV electrons by thin foils," Med. Phys. **35**, 4121–4131 (2008).

[12] www.graphitestore.com.

[13]F. McCarthy, V. Sahajwalla, J. Hart, and N. Saha-Chaudhury, "Influence of ash on interfacial reactions between coke and liquid iron," Metal. Mater. Trans. B **34B**, 573–580 (2003).

[14]www.goodfellow.com.

[15]B. R. Archer, P. R. Almond, and L. K. Wagner, "Application of a Laplace transform pair model for high energy x-ray spectral reconstruction," Med. Phys. **12**, 630–633 (1985).

[16]M. R. McEwen, "Measurement of ionization chamber absorbed dose k_Q factors in megavoltage photon beams," Med. Phys. **37**, 2179–2193 (2010).

[17]M. McEwen and C. Ross, "Unexpected doserate dependencies of diodes for beam scanning," Med. Phys. **35**, 2920 (2008) (abstract).

[18]A. Piermattei, G. Arcovito, L. Azario, C. Bacci, L. Bianciardi, E. De Sapio, and C. Giacco, "A study of quality of bremsstrahlung spectra reconstructed from transmission measurements," Med. Phys. **17**, 227–233 (1990).

[19]P.-H. Huang, K. R. Kase, and B. E. Bjärngard, "Spectral characterization of 4 MV bremsstrahlung by attenuation analysis," Med. Phys. **8**, 368–374 (1981).

[20]S. D. Ahuja, P. G. Steward, T. S. Roy, and E. D. Slessinger, "Estimated spectrum of a 4-MV therapeutic beam," Med. Phys. **13**, 368–373 (1986).

[21]A. Piermattei, G. Arcovito, F. A. Bassi, and L. Azario, "Reconstruction of 9 MV bremsstrahlung spectrum by numerical analysis of measured transmission data," Physica Medica **1**, 43–57 (1987).

[22]T. Shimozato, K. Tabushi, S. Kitoh, Y. Shiota, C. Hirayama, and S. Suzuki, "Calculation of 10 MV x-ray spectra emitted by a medical linear accelerator using the BFGS quasi-Newton method," Phys. Med. Biol. **52**, 515–523 (2007).

[23]J. P. McCaffrey, B. Downton, H. Shen, D. Niven, and M. McEwen, "Pre-irradiation effects on ionization chambers used in radiation therapy," Phys. Med. Biol. **50**, N121–N133 (2005).

[24]P. R. Almond, P. J. Biggs, B. M. Coursey, W. F. Hanson, M. S. Huq, R. Nath, and D. W. O. Rogers, "AAPM's TG-51 protocol for clinical reference dosimetry of high-energy photon and electron beams," Med. Phys. **26**, 1847–1870 (1999).

[25]J. P. Seuntjens, C. K. Ross, K. R. Shortt, and D. W. O. Rogers, "Absorbed-dose beam quality conversion factors for cylindrical chambers in high-energy photon beams," Med. Phys. **27**, 2763–2779 (2000).

[26]R. E. Bentley, *Uncertainty in Measurement: The ISO Guide*, 6th ed. (National Measurement Laboratory CSIRO, Australia, 2003).

[27]N. Takata and Y. Morishita, "Effect of radiation-induced charge accumulation on build-up cap on the signal current from an ionisation chamber," Radiat. Prot. Dosim. **145**, 21–27 (2011).

[28]D. W. O. Rogers, B. A. Faddegon, G. X. Ding, C.-M. Ma, J. Wei, and T. R. Mackie, "BEAM: A Monte Carlo code to simulate radiotherapy treatment units," Med. Phys. **22**, 503–524 (1995).

[29]D. W. O. Rogers, B. Walters, and I. Kawrakow, "BEAMnrc Users Manual," NRC Technical Report PIRS-509(A) revL (National Research Council of Canada, Ottawa, Canada, 2011) (available URL: http://www.irs.inms.nrc.ca/BEAM/beamhome.html).

[30]I. Kawrakow, D. W. O. Rogers, and B. Walters, "Large efficiency improvements in BEAMnrc using directional bremsstrahlung splitting," Med. Phys. **31**, 2883–2898 (2004).

[31]I. Kawrakow, E. Mainegra-Hing, F. Tessier, and B. R. B. Walters, "The EGSnrc C++ class library," Technical Report PIRS-898 (rev A) (National Research Council of Canada, Ottawa, Canada, 2009) (available URL: http://www.irs.inms.nrc.ca/EGSnrc/PIRS898/).

[32]B. R. Muir and D. W. O. Rogers, "Monte Carlo calculations of k_Q, the beam quality conversion factor," Med. Phys. **37**, 5939–5950 (2010).

[33]F. Tessier and I. Kawrakow, "Calculation of the electron-electron bremsstrahlung cross-section in the field of atomic electrons," Nucl. Inst. Meth. B **266**, 625–634 (2008).

[34]I. Kawrakow, "Electron impact ionization cross sections for EGSnrc," Med. Phys. **29**, 1230 (2002) (abstract).

[35]IAEA, "Handbook of photonuclear data for applications: Cross sections and spectra," Technical Report TECDOC 1178 (Vienna, Austria, IAEA, 2000) (available URL: http://www-nds.iaea.org/photonuclear).

[36]E. S. M. Ali and D. W. O. Rogers, "Implementation of photonuclear attenuation in EGSnrc," *Technical report CLRP 12-01* (Carleton University, Ottawa, Canada, 2012), 14 pp., available URL: http://www.physics.carleton.ca/clrp/photonuclear.

[37]H. W. Koch and J. W. Motz, "Bremsstrahlung cross-section formulas and relate.d data," Rev. Mod. Phys. **31**, 920–955 (1959).

[38]B. A. Faddegon, M. Asai, J. Perl, C. Ross, J. Sempau, J. Tinslay, and F. Salvat, "Benchmarking of Monte Carlo simulation of bremsstrahlung from thick targets at radiotherapy energies," Med. Phys. **35**, 4308–4317 (2008).

[39]B. R. Muir, M. R. McEwen, and D. W. O. Rogers, "Beam quality conversion factors for parallel-plate ionization chambers in MV photon beams," Med. Phys. **39**, 1618–1631 (2012).

[40]J. Borg, I. Kawrakow, D. W. O. Rogers, and J. P. Seuntjens, "Experimental verification of EGSnrc Monte Carlo calculated ion chamber response in low energy photon beams," in *Proceedings of the 22nd Annual International Conference of IEEE Engineering in Medicine and Biology Society* (IEEE, Chicago, IL, 2000), Vol. 4, pp. 3152–3155.

[41]J. P. Seuntjens, I. Kawrakow, J. Borg, F. Hobeila, and D. W. O. Rogers, "Calculated and measured air-kerma response of ionization chambers in low and medium energy photon beams," in *Proceedings of an International Workshop on Recent Developments in Accurate Radiation Dosimetry*, edited by J. P. Seuntjens and P. Mobit (Medical Physics Publishing, Madison, WI, 2002), pp. 69–84.

[42]B. R. Muir, M. R. McEwen, and D. W. O. Rogers, "Measured and Monte Carlo calculated k_Q factors: Accuracy and comparison," Med. Phys. **38**, 4600–4609 (2011).

[43]J. H. Hubbell, "Review of photon interaction cross section data in the medical and biological context," Phys. Med. Biol. **44**, R1–R22 (1999).

[44]I. Kawrakow, "Accurate condensed history Monte Carlo simulation of electron transport. II. Application to ion chamber response simulations," Med. Phys. **27**, 499–513 (2000).